Steel and Composite Structures, *Vol. 54, No. 4 (2025) 331-344*
https://doi.org/10.12989/scs.2025.54.4.331

Seismic performance of concrete-filled hollow precast concrete columns with prefabricated inner mold

Chae-Rim Im[1a], Sanghee Kim*[2], Ju-Hyun Mun[2b], Keun-Hyeok Yang[2c], and Jae-Il Sim[3d]

[1]Department of Architectural Engineering, Kyonggi University, Graduate School, Suwon, Republic of Korea
[2]Department of Architectural Engineering, Kyonggi University, Suwon, Republic of Korea
[3]Korea Disaster Prevention Safety Technology Co. Ltd, Gwangju, Republic of Korea

(Received March 18, 2024, Revised May 13, 2024, Accepted August 13, 2024)

Abstract. In this experimental study, cyclic loading tests were conducted to evaluate the seismic performance of concrete-filled hollow precast concrete (PC) columns (HPCC) manufactured using an inner mold composed of shear studs and louver plates. Both shear studs and louver plates were employed to ensure the structural integrity between the old concrete (outer shell) and new concrete (cast-in-place concrete). The hollow ratio of the test specimens fabricated using the inner mold was 22%. Up to a drift ratio of 3.0%, the hysteresis loops, yielding stiffnesses, and dissipated energies of the hollow column specimens were nearly identical to those of the monolithic columns. Beyond the peak strength, the hollow specimens—monolithically connected to the foundation—exhibited a lower hysteresis loop, dissipated energy, and displacement ductility ratio than the monolithic column specimens; this trend was more pronounced in the PC specimens with sleeve connections. The strain histories of the longitudinal bars of all the specimens were nearly identical, regardless of the presence of a hollow section. All the column specimens exhibited a measured peak moment exceeding the nominal peak moment in accordance with the ACI 318 standard. Overall, the HPCC specimens fabricated using the proposed prefabricated inner mold exhibited structural behavior similar to that of conventional RC columns.

Keywords: hollow PC column; precast concrete column; reinforced concrete column; seismic performance; steel stud

1. Introduction

Domestic and international construction industries face significant challenges in assembling rebar and casting concrete components on site owing to labor shortages and aging skilled workers. To address these challenges, precast concrete (PC) construction has been increasingly adopted, a method in which concrete components are manufactured in a factory and transported to a construction site for assembly (Hajdukiewicz *et al*. 2016, Kim *et al*. 2021, Jung *et al*. 2023). PC construction enhances the productivity and quality of concrete components via factory production, thus shortening the construction period and potentially leading to overall cost savings. Hollow precast concrete columns (HPCC) are being developed to ensure the economic viability of PC construction and ease of transportation and installation (Im *et al*. 2023a, Jin *et al*. 2023, Wang *et al*. 2023a). HPCC involves assembling a component onsite by casting concrete into a hollow section produced in a factory. This hollow section helps reduce the weight of the PC member, thus offering advantages for transportation, lifting, and assembly. However, a persistent issue with HPCC is the compromised integrity between factory-produced concrete and onsite-cast concrete (Hwang *et al*. 2016, Hao *et al*. 2022, Ke *et al*. 2023). Additionally, manufacturing the inner mold, which creates a hollow section, poses challenges owing to the use of cross-ties as inner transverse reinforcements.

Kim *et al*. (2016) evaluated the seismic performances of HPCCs assembled using precast PC panels and those assembled using saddle-shaped ties. HPCCs employing saddle-shaped ties had an initial stiffness and maximum internal forces similar to those of monolithic RC columns, although their ductility and energy-dissipation capacity were somewhat lower. In contrast, HPCCs assembled with PC panels secured the integrity between the new and old concrete using diagonal ties and transverse confinement, thus achieving a lateral load-displacement relationship and energy dissipation capacity comparable to those of monolithic RC columns.

Yang *et al*. (2018) evaluated the seismic behavior of an inner mold made of high-strength bolts and tear plates to secure the structural integrity between the new and old concrete in a hollow column. The test results revealed that bonding cracks occurred between the inner mold and old concrete, with the measured bending moment being lower than the predicted bending moment. Wang *et al*. (2023b) evaluated the bending behavior of hollow columns that secured the integrity between new and old concrete by welding stiffeners inside a concrete-filled steel tube. Columns with stiffeners inside the steel tube exhibited a

*Corresponding author, Ph.D. Assistant Professor
E-mail: sanghee0714@kyonggi.ac.kr
[a]Graduate Student
[b]Ph.D. Associate Professor
[c]Ph.D. Professor
[d]Ph.D. CEO

http://www.techno-press.com/journals/scs&subpage=8
ISSN: 1229-9367 (Print), 1598-6233 (Online)

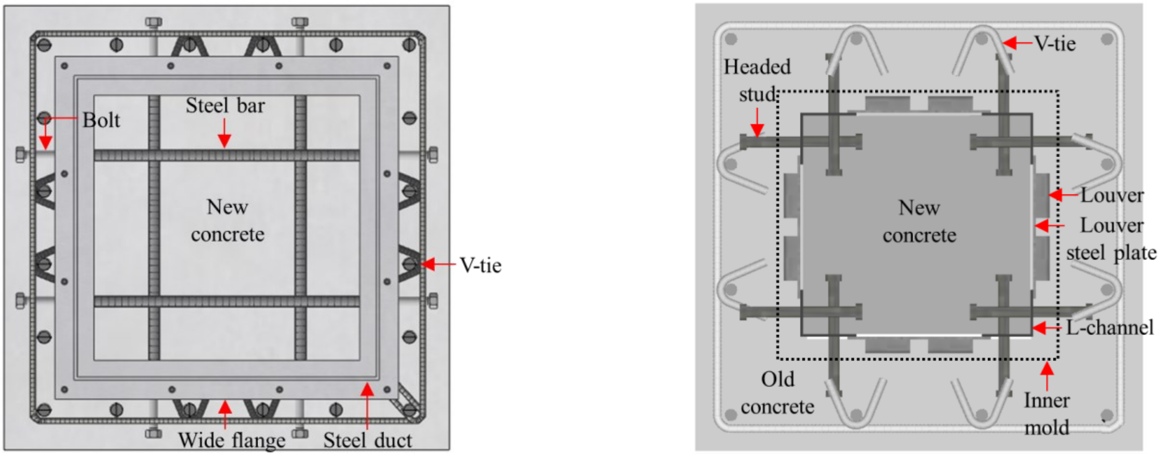

(a) Previous study (left) (Im *et al*. 2023a) and new inner mold (right)

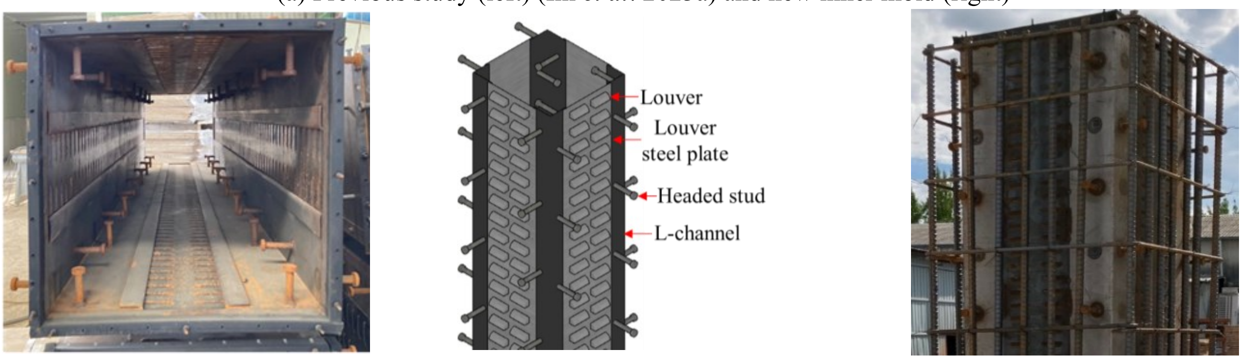

(b) Inner mold of hollow core PC column

Fig. 1 Schematic of prefabricated inner mold for HPCC

maximum internal force similar to that of monolithic columns, approximately 1.03 times, although their displacement ductility ratio decreased by approximately 19.1%. Im *et al*. (2023a) conducted quasi-static cyclic loading tests to evaluate the seismic performance of HPCCs using steel ducts or rubber tubes to form hollow sections. The maximum bending moments of the specimens using steel ducts or rubber tubes satisfied the predicted moments according to ACI 318 (2019). In the lateral load–displacement relationship, the load reduction magnitude after reaching the peak internal forces in the HPCC specimens was slightly higher than that in the solid specimens. The structural behavior of the HPCC specimens fabricated using steel ducts or rubber tubes was similar to that of the solid columns.

In this study, an improved technique for efficiently producing HPCC was proposed based on a previous study (Im *et al*. 2023a), wherein steel ducts were used to form hollow sections and improved details were proposed to improve the structural integrity between new and old concrete in HPCCs. Nevertheless, there are difficulties in using steel bars that penetrate the steel duct and connect the steel ducts individually with bolts (Im *et al*. 2023a). Thus, the key feature of the improved HPCC in this study is the simplified formation of the hollow section, achieved by eliminating the steel bars that penetrate and cross the inner mold. Additionally, the improved HPCC aims to ensure the structural integrity between the new and old concrete by using shear studs and louver plates and to reduce amount of transverse reinforcement by using V-ties (Fig. 1). The prefabricated inner mold comprised shear studs, L-channels, and louver plates. Shear studs were attached to the inside and outside of the L-channels to ensure the structural integrity between the outer shell concrete and the cast-in-place core concrete. According to the results of the push-out tests conducted by Im *et al*. (2023b), the combination of shear studs and louver plates can significantly increase the shear strength. Additionally, instead of removing the cross-ties, V-ties were used to prevent buckling of the longitudinal bars and to reduce amount of transverse reinforcement. Quasi-static cyclic loading tests were conducted to assess the structural performance of the newly designed HPCC using a prefabricated inner mold, with its failure mode, strength, ductility, and energy dissipation performance compared with that of a conventional RC column.

2. Experiment investigation

2.1 Test specimens

In this experimental study, five specimens were produced to assess the seismic performance of the HPCCs using the proposed prefabricated inner mold: one specimen was a conventional RC column, while the other four were HPCC specimens with various variables. Table 1 summarizes and compares the details and variables of all

Table 1 Specimen details

Specimens	Connector type	Shear connector type	Hollow ratio (%)	A_g (mm^2)	A_h (mm^2)	L (mm)	f_c (MPa)	s (mm)	ω	ρ_{vh}	ρ_s	M_n (kN-m)	W_c (kg)
CTRL	-	-	-	360000	-	2400	24	250	1.04	0.02	0.02	679	2795
CTRL-PC	Sleeve												2643
HC-24	-	Louver steel plate + Headed stud	22		78400								2718
HC-24-PC	Sleeve												2607
HC-50	-						50	125	1.0	0.04		772	3288

* A_g: total sectional area of column; A_h: hollow sectional area of column; L: length from interface between column and bottom foundation to lateral loading point; f_c: designed compressive strength; s: spacing of transverse column transverse confinement; ω: ratio of provided to required transverse reinforcement in accordance with ACI 318-19, calculated using specific material properties; ρ_{vh}: volumetric transverse reinforcing bar ratio; ρ_s: longitudinal reinforcing bar ratio; M_n: calculated nominal moment based on specific material properties; and W_c: weight of column specimen excluding foundation.

five specimens, whereas Fig. 2 depicts the dimensions and reinforcement details of the specimens. The main experimental variables were the presence of a hollow section, compressive strength of the concrete, and details of the column-foundation connection.

All the specimens had a total cross-sectional area of 600 × 600 mm², and the height (L) from the concrete base to the loading point was 2400 mm. The hollow ratio of the hollow columns was 22%. The design compressive strength (f'_c) was set to either 24 MPa or 50 MPa, and the f'_c values of the precast outer shell and site-cast concrete filling the hollow section were the same.

CTRL-series: The CTRL-series specimens were conventional and precast RC columns without hollow sections. The longitudinal reinforcing bar ratio (ρ_s) of the control specimen (CTRL) was about 0.02. To achieve this ratio, sixteen SD500 D22 [d_b = 22 mm] column longitudinal bars were used, where SD500 is the steel nominal strength (f_y) of 500 MPa and d_b is the diameter of the steel bar. The transverse reinforcing bars were SD500 D13 [d_b = 13 mm] and arranged as one closed hoop and three cross-ties each way. The spacing (s) of the transverse confinement was 250 mm, and the spacing was 125 mm (= s/2) from the top face of the concrete base up to 600 mm in accordance with ACI 318. The volumetric transverse reinforcing bar ratio (ρ_{vh}) with the spacing of 250 mm was approximately 0.02. The concrete cover was 60 mm thick. Here, the CTRL-PC specimen had the same cross-sectional details as the CTRL specimen and was an experimental setup in which the longitudinal bars of a precast column produced in a factory were connected to the foundation's dowel bars with a sleeve. The nominal moment strength (M_n) of both specimens was 679 kN-m.

HC-series: HC-series specimens were produced using a prefabricated inner mold to create the outer shell concrete, followed by casting the cast-in-place (CIP) concrete into the hollow section (Fig. 2). The inner mold, designed to create the hollow section, was fabricated by welding L-channels and louver plates together, measuring 280 × 280 × 2700 mm³. The L-channels, crafted from 3-mm-thick steel plates through cold forming, had dimensions of 100 × 100 mm. The louver steel plates, 1.6 mm in thickness, featured louvers sized 15 × 80 mm² and 2 mm in height, spaced 45 mm apart (Fig. 2(f)). Headed studs were welded to the L-channels to bolster the structural integrity and promote bonding between the new and old concrete. These studs, with diameters of 16 mm and lengths of 80 mm, were installed both inside and outside the mold at 150 mm intervals.

The longitudinal bars of the HC-24 specimen were arranged in the same manner as those of the CTRL specimen using sixteen SD500 D22 bars. For transverse confinement, hoops of SD500 D13 were placed at 250 mm spacing, with bent V-ties installed instead of inner cross-ties. The type of V-tie used was SD500 D13 with a length and bending angle of 72° and 45°, respectively. The design of the V-ties followed that of Kim and Yang (2015). The HC-24-PC specimen had the same cross-sectional details as the HC-24 specimen, with the longitudinal reinforcing bars and the foundation's dowel bars connected using splice sleeves.

The HC-50 specimen was identical to the HC-24 specimen in all aspects except for concrete strength and transverse confinement. The f'_c value of the HC-50 specimen was 50 MPa, indicating relatively high strength, while the spacing (s) of the transverse confinement was 125 mm. The volumetric transverse reinforcing bar ratio (ρ_{vh}) of the HC-50 specimen was 0.04, and the nominal moment strength (M_n) was 772 MPa.

2.2 Material properties

The f'_c values for the column specimens were 24 MPa and 50 MPa. To measure the compressive strength of the concrete, three ϕ100 × 200 mm cylinders were prepared for each specimen on the day of casting, with compressive tests performed in accordance with ASTM C39/C39M (2020). Table 2 lists the average measured compressive strengths ($f'_{c\text{-}me}$) of the concrete used for each specimen. For specimens with f'_c of 24 MPa, $f'_{c\text{-}me,out}$ and $f'_{c\text{-}me,in}$ were 25.1 MPa and 24.2 MPa, respectively; for specimens with f'_c of 50 MPa, they were 46.0 MPa and 45.1 MPa, respectively.

To evaluate the properties of the steel materials used in the specimens, three samples were prepared for each type of steel, with tensile tests conducted in accordance with ASTM E8/E8M (2016). The results of the tensile tests are

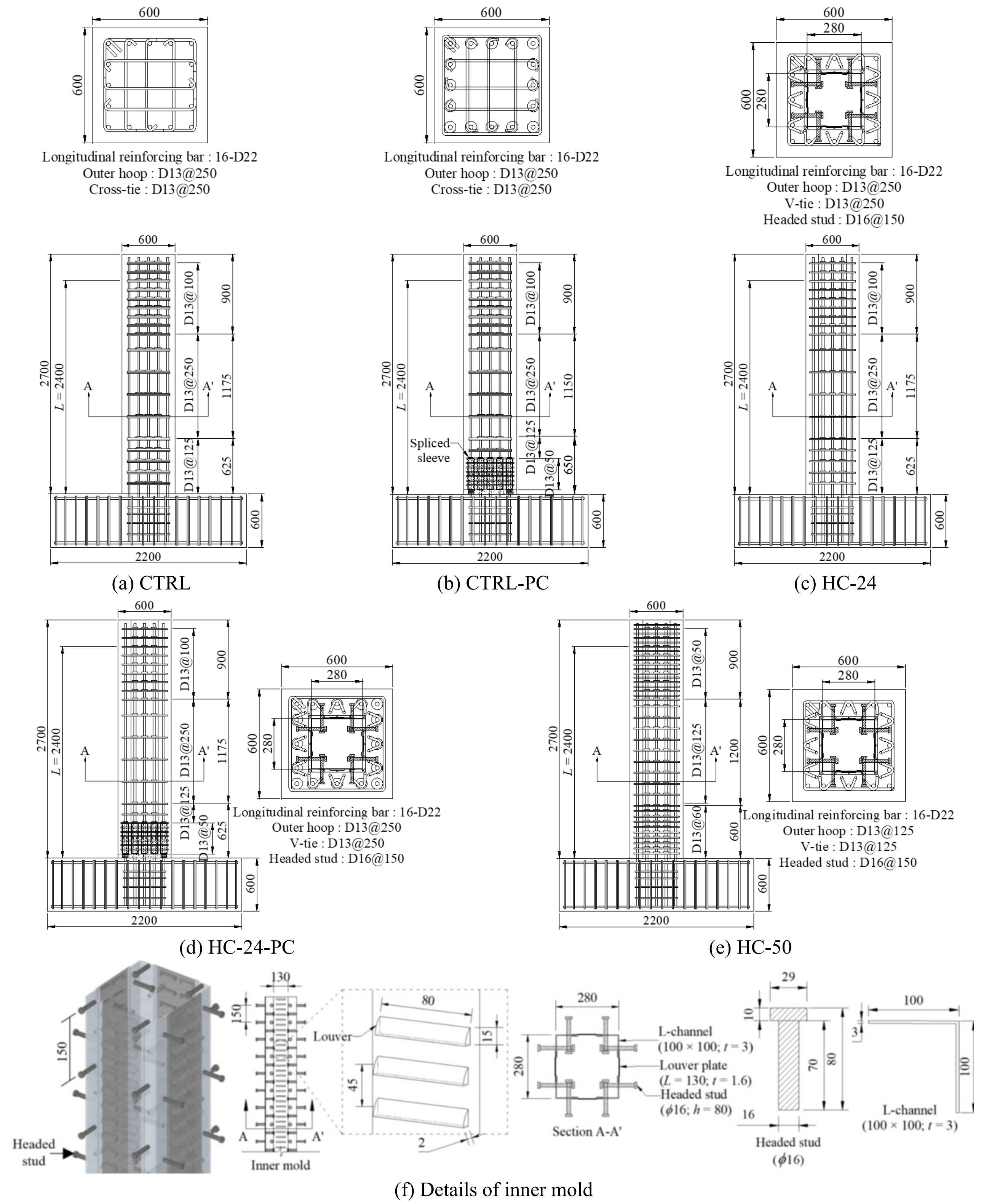

Fig. 2 Parameters of column specimens (units: mm)

presented in Table 3 and Fig. 3. The measured yield strengths of SD500 D13 and SD500 D22 were 531 MPa and 553 MPa, respectively. The measured yield strengths for the SM355 used in the L-channels and louver plates were 247 and 334 MPa, respectively. The yield strength of headed studs was 213 MPa.

2.3 Test setup

Lateral cyclic loading tests on the columns were conducted using a 2000 kN actuator to apply repeated lateral loads to the top of the columns (Fig. 4). The repeated loading followed the ACI 374.1 (2019) guidelines, utilizing

Table 2 Mechanical properties of concrete

f_c (MPa)	$\rho_{c\text{-}me,out}$ (kg/m^3)	$\rho_{c\text{-}me,in}$ (kg/m^3)	$f'_{c\text{-}me,out}$ (MPa)	$f'_{c\text{-}me,in}$ (MPa)	$E_{c\text{-}me,out}$ (MPa)	$E_{c\text{-}me,in}$ (MPa)	$\varepsilon_{c\text{-}me,in}$	$\varepsilon_{c\text{-}me,out}$
24	2205	2210	25.1	24.2	23585	23220	0.0024	0.0024
50	2232	2229	46.0	45.1	34120	30974	0.0025	0.0026

* $\rho_{c\text{-}me,out}$: unit weight of concrete in the outside column, $\rho_{c\text{-}me,in}$: unit weight of concrete in the inside column, $f'_{c\text{-}me,out}$: compressive strength of concrete in the outside column, $f'_{c\text{-}me,in}$: compressive strength of concrete in the inside column, $E_{c\text{-}me,out}$: elastic modulus of concrete in the outside column, $E_{c\text{-}me,in}$: elastic modulus of concrete in the inside column, $e_{c\text{-}me,in}$: strain at peak stress of concrete in the outside column, and $e_{c\text{-}me,out}$: compressive strength of concrete in the inside column.

Table 3 Mechanical properties of steel coupons

Steel type	Yield strength (MPa)	Tensile strength (MPa)	Yield strain	Elastic modulus (MPa)
SD500 D13	531	658	0.0026	201834
SD500 D22	553	691	0.0026	211321
L-channel	247	339	0.0015	165204
Louver plate	334	442	0.0020	169752
Headed stud	213	415	0.0028	76056

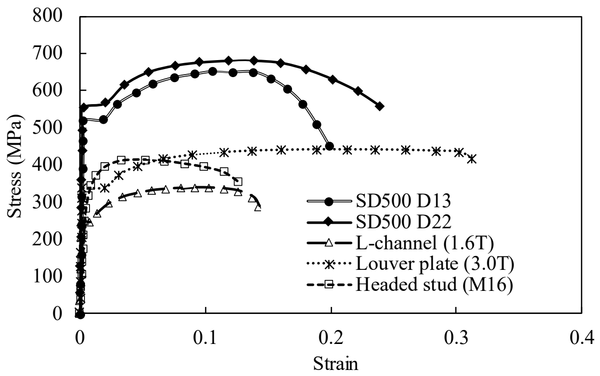

Fig. 3 Strain-stress curve of steel material used for the specimens

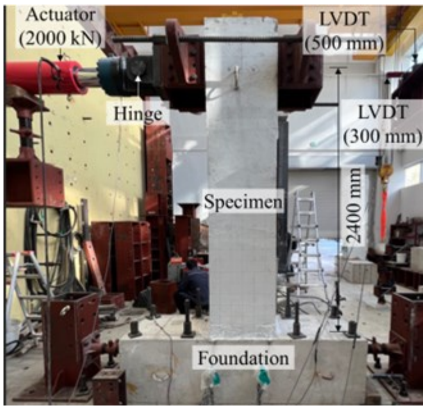

Fig. 4 Test setup

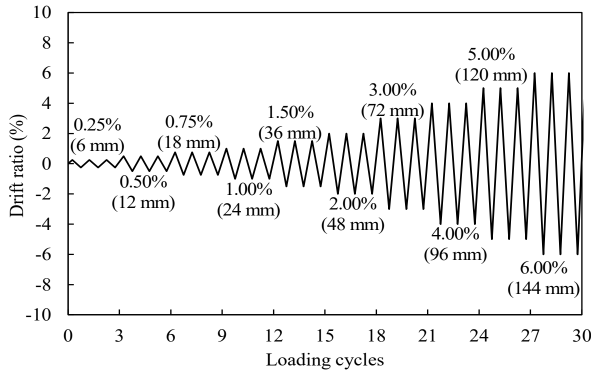

Fig. 5 Loading Cycle of ACI 374.1

the displacement control method and executing three cycles per target drift ratio (Fig. 5). During the tests, the columns were not subjected to axial loading. Linear variable differential transducers (LVDTs) with capacities of 300 and 500 mm were placed at the loading points to measure the lateral displacement. The concrete foundation was firmly anchored to a strong floor using rock bolts with a diameter of 50 mm. A steel frame was positioned to prevent the toppling of the specimen during repeated loading.

3. Test results

3.1 Failure mode

Figure 6 shows the crack propagation and failure modes for each specimen. The initial cracks in the CTRL specimen appeared in the lower part of the specimen at a drift ratio of 0.25% before gradually extending upward as the lateral displacement increased (Fig. 6(a)). At a drift ratio of 3%, the external concrete layer at the lower part of the specimen started to spall, leading to complete failure at a drift ratio of 7.0% owing to extensive spalling of the outer layer, buckling of the longitudinal reinforcement, and loosening of the internal cross-ties.

The initial cracks in the CTRL-PC specimen appeared at the same drift ratio of 0.25% as that in the CTRL specimen (Fig. 6(b)). At the point of peak force, cracks that formed in the lower section of the test area resulted in spalling of the external concrete layer at a drift ratio of 3%. The CTRL-PC specimen ultimately failed at a drift ratio of 6% owing to the fracture of the longitudinal reinforcement beneath the sleeve, where the gap was between the column and foundation.

The initial cracks in the HC-24 specimen appeared at the same drift ratio of 0.25% as those in the CTRL specimen, with the spalling of the outer concrete layer at the specimen ends occurring at a drift ratio of 3% (Fig. 6(c)). The specimen ultimately failed at a drift ratio of 7.0% because of buckling of the longitudinal reinforcement and fracture

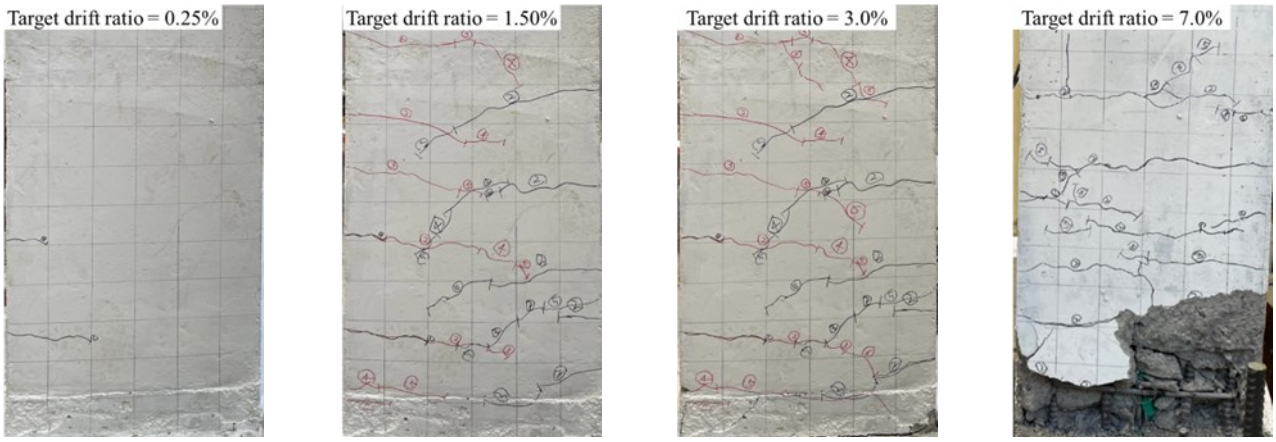

At Δ_{cr} (0.25%) At Δ_y (1.50%) At Δ_{peak} (3.0%) At failure (7.0%)

(a) CTRL

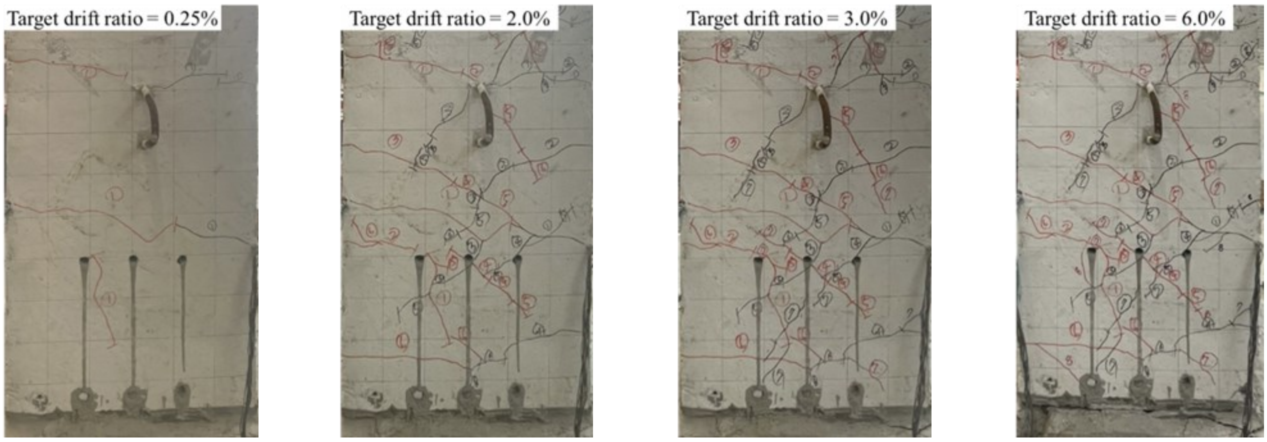

At Δ_{cr} (0.25%) At Δ_y (2.0%) At Δ_{peak} (3.0%) At failure (6.0%)

(b) CTRL-PC

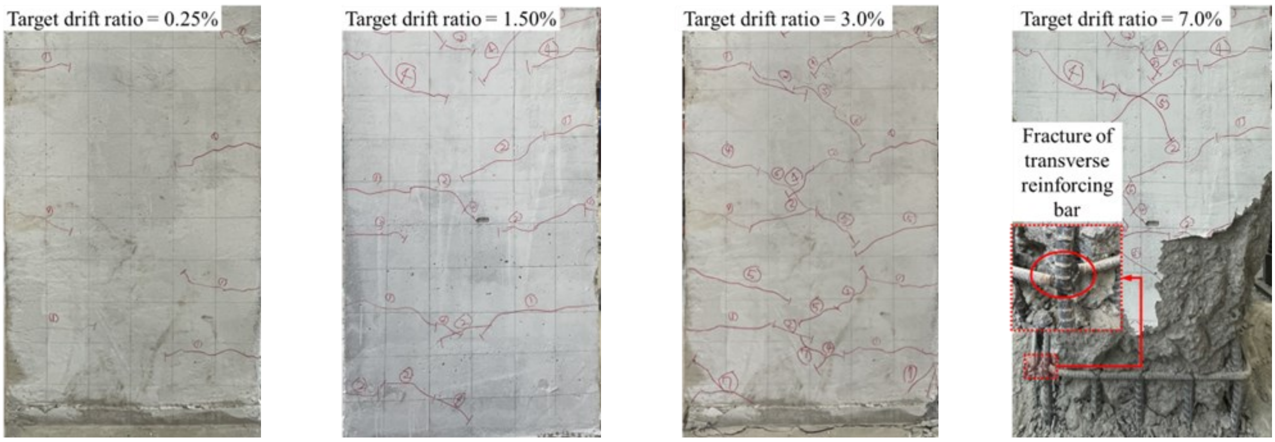

At Δ_{cr} (0.25%) At Δ_y (1.50%) At Δ_{peak} (3.0%) At failure (7.0%)

(c) HC-24 (continued)

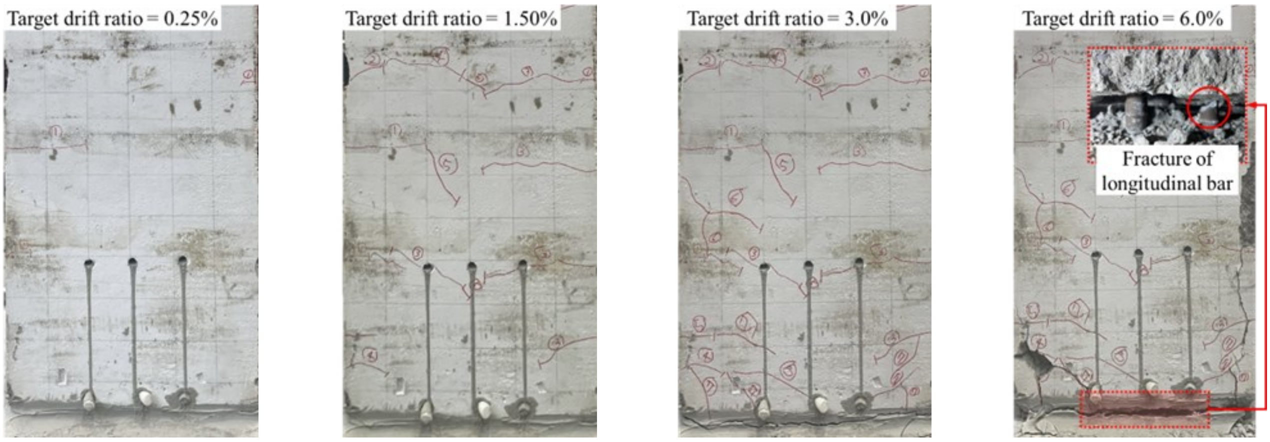

At Δ_{cr} (0.25%) At Δ_y (1.50%) At Δ_{peak} (3.0%) At failure (6.0%)

(d) HC-24-PC

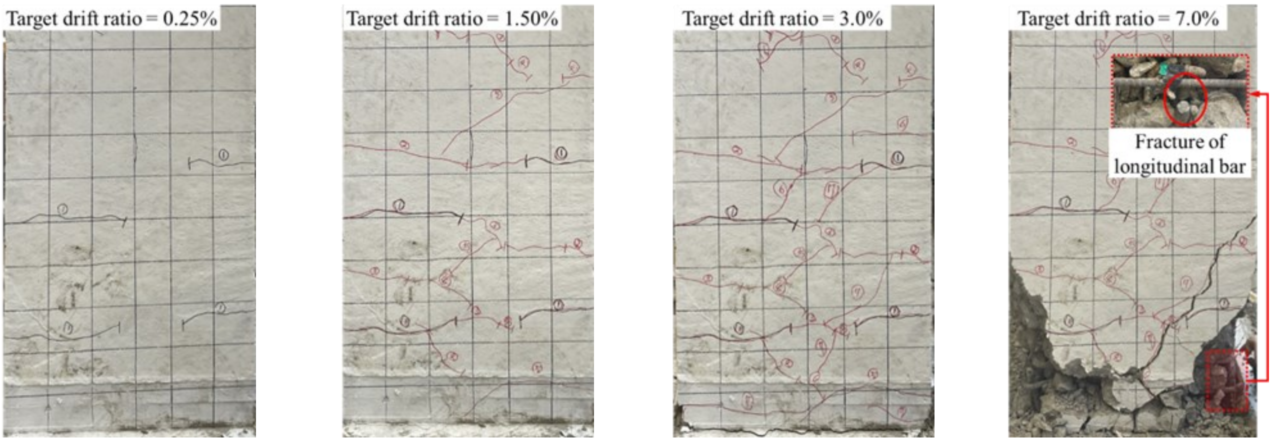

At Δ_{cr} (0.25%) At Δ_y (1.50%) At Δ_{peak} (3.0%) At failure (7.0%)

(e) HC-50

Fig. 6 Cracks propagation of columns

of the hoop. There was no fracture of the longitudinal reinforcement or loosening of the transverse confinement. In our findings, the HC-24 specimen exhibited fewer flexural cracks compared to the CTRL specimen. This difference can be attributed to the reduced shear friction at the interface between the steel plate and concrete, as compared to the shear friction resulting from the interlocking of concrete aggregates. Consequently, the load transfer capacity within the column cross-section was diminished, leading to a concentration of stress and the formation of crack surfaces in specific areas.

The initial cracks in the HC-24-PC specimen occurred at a drift ratio of 0.25% (Fig. 6(d)). The subsequent behavior was similar to that of the CTRL-PC specimen. Spalling of the outer concrete layer at the specimen ends occurred at a drift ratio of 3%, and the specimen ultimately failed because of the fracture of the longitudinal reinforcement beneath the sleeve at a drift ratio of 6.0%. Additionally, the HC-24-PC specimen exhibited fewer cracks progressing upward than the other specimens, attributed to the stress concentration caused by the sleeve, which led to steel bar fracture, potentially resulting in brittle failure. The HC-24-PC specimen exhibited fewer flexural cracks compared to the CTRL-PC specimen. This outcome, similar to that observed in the HC-24, is attributed to the decreased shear friction at the interface between the steel plate and concrete.

The initial cracks in the HC-50 specimen occurred at the same drift ratio of 0.25% as in the other specimens (Fig. 6(e)). At the point of maximum force, cracks that appeared in the lower part of the test section led to the spalling of the outer concrete layer at a drift ratio of 3%. The specimen ultimately failed at a drift ratio of 7.0% owing to an expanded range of spalling in the outer concrete layer at the lower part and the fracture of the longitudinal bar.

3.2 Lateral load and displacement relationships

Table 4 summarizes the experimental results. Yielding displacement (Δ_y), yielding strength (P_y), and ductility ratio (μ_Δ) are defined using an equivalent elastoplastic system with secant stiffness at $0.75P_{peak}$ (Fig. 7). The ultimate displacement corresponds to $0.8P_{peak}$ after reaching the maximum load. In Table 4, ratio of provided to required transverse reinforcement in accordance with ACI 318-19 (ω^*) is the ratio of the provided to required transverse reinforcement in accordance with ACI 318-19, calculated using the measured material properties, and all values of ω^* were similar to the design ratio of provided to required

Table 4 Test result

Speci-mens	ω^*	P_{cr} (kN)	P_y (kN)	P_{peak} (kN)	M_{peak} (kN-m)	Δ_{cr} (mm) [%]	Δ_y (mm) [%]	Δ_{peak} (mm) [%]	Δ_u (mm) [%]	K_y (kN/m)	K_p (kN/m)	μ_Δ	E_{acc} (kN·m)	ξ_D (%)	M^*_n (kN-m)	M_{peak}/M^*_n
CTRL	1.06	128.3	291.6	388.8	933.1	6.0 [0.25]	30.5 [1.3]	72.3 [3.0]	144.0 [6.0]	9.56	2.70	4.72	534.9	18.7	734	1.27
CTRL-PC	1.06	125.5	285.2	380.2	912.5	6.0 [0.25]	39.9 [1.7]	72.3 [3.0]	144.0 [6.0]	7.15	2.64	3.61	423.6	12.4	734	1.24
HC-24	1.06	128.1	291.1	392.5	942.0	6.0 [0.25]	30.5 [1.3]	72.3 [3.0]	144.0 [6.0]	9.54	2.70	4.72	590.3	17.5	734	1.28
HC-24-PC	1.06	111.7	254.0	338.8	813.1	6.0 [0.25]	33.5 [1.4]	72.1 [3.0]	120.3 [5.0]	7.58	2.81	3.59	338.9	15.9	734	1.11
HC-50	1.16	131.8	299.6	415.4	997.0	6.0 [0.25]	36.0 [1.5]	72.2 [3.0]	152.0 [6.3]	8.32	2.63	4.22	681.0	23.6	807	1.24

* ω^*: ratio of provided to required transverse reinforcement in accordance with ACI 318-19, calculated using measured material properties; P_{cr}: initial cracking load; P_y: load at yielding; P_{peak}: peak load; M_{peak}: maximum moment capacity; Δ_{cr}: displacement at initial cracking; Δ_y: displacement at yielding; Δ_{peak}: displacement at peak load; Δ_u: displacement at $0.8P_{peak}$ after P_{peak}; K_y: secant stiffness at yielding; K_{peak}: secant stiffness at peak load: μ_Δ: displacement ductility ratio; E_{acc}: cumulative dissipated energy from the first drift ratio to $0.8P_{peak}$ after P_{peak}; ξ_D: equivalent damping ratio; and M^*_n: calculated moment strength based on measured material properties.

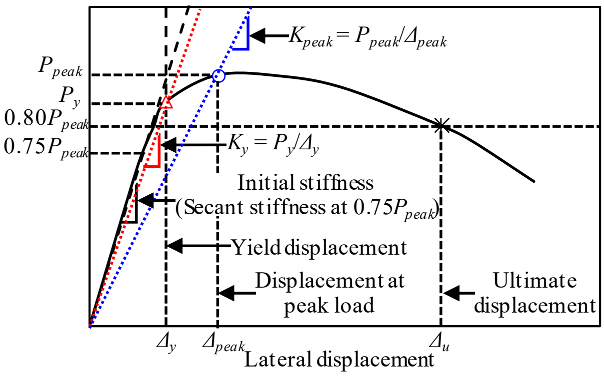

Fig. 7 Definitions of yield and ultimate displacements

transverse reinforcement in accordance with ACI 318-19 (ω) provided to the required transverse reinforcement. M^*_n is calculated moment strength based on the measured material properties, and all values of M^*_n were similar to the nominal moment strength obtained from experimental results (M_n).

Fig. 8 depicts the hysteretic lateral load-displacement relationship for each specimen, and the important points are highlighted in the graph. The initial cracking load (P_{cr}) of the CTRL specimen was 128 kN at a drift ratio of 0.25% (displacement of 6.0 mm). P_y was measured as 292 kN at a drift ratio of 1.25% (displacement of 30.5 mm). P_{peak} was measured as 389 kN at a drift ratio of 3.0% (displacement of 72.0 mm). After reaching the peak, the load gradually decreased. The experiment ended at a drift ratio of 7% owing to the loosening of the internal transverse reinforcement, and at that time, the lateral load was approximately 58% of P_{peak} or 225 kN.

The initial cracking load (P_{cr}) of the CTRL-PC specimen was 126 kN at a drift ratio of 0.25% (displacement of 6.0 mm). P_y was measured as 285 kN at a drift ratio of 1.64% (displacement of 39.9 mm). P_{peak} was measured to be 380 kN at a drift ratio of 3.0% (displacement of 72 mm). The main reinforcement fractured beneath the splice sleeve at a drift ratio of 6.0% (displacement of 144 mm), and the lateral load was 65% of P_{peak} or 246 kN. P_{cr}, P_y, and P_{peak} were approximately 2.2% lower than those of the CTRL specimen, and the rate of load decrease after the peak was slightly more pronounced than that of the CTRL specimen.

The initial cracking load (P_{cr}) of the HC-24 specimen was measured to be 128 kN at a drift ratio of 0.25% (displacement of 6.0 mm). P_y was measured as 291 kN at a drift ratio of 1.25% (displacement of 30.5 mm). P_{peak} was measured to be 393 kN at a drift ratio of 3.0% (displacement of 72.0 mm); these measurements were comparable to those of the CTRL and CTRL-PC specimens. The HC-24 specimen experiment ended because of a sudden load drop caused by the fracture of the outer hoop; the drift ratio at that time was 7.0%, and the lateral load was 47% of P_{peak} or 184 kN. In addition, the rate of load decrease in the post-peak load phase of the HC-24 specimen was similar to that of the CTRL-PC specimen.

The initial cracking load (P_{cr}) of the HC-24-PC specimen was 112 kN at a drift ratio of 0.25% (displacement of 6.0 mm). P_y was measured as 254 kN at a drift ratio of 1.40% (displacement of 33.5 mm). P_{peak} was measured to be 339 kN at a drift ratio of 3.0% (displacement of 72.0 mm). These values were 11% and 14% lower than those of the CTRL-PC and HC-24 specimens, respectively. Similar to the CTRL-PC specimen, the HC-24-PC experiment ended because of a sudden load drop caused by the fracture of the main reinforcement beneath the splice sleeve. The drift ratio was 6.0%, and the lateral load was 26% of P_{peak}, i.e., 88 kN. Moreover, the HC-24-PC specimen showed a much more significant decrease in load after the peak than the CTRL-PC and HC-24 specimens.

The initial cracking load (P_{cr}) of the HC-50 specimen was measured as 132 kN with a drift ratio of 0.25% (displacement of 6.0 mm). P_y was measured as 300 kN at a drift ratio of 1.50% (displacement of 36.0 mm). P_{peak} was measured to be 415 kN at a drift ratio of 3.0% (displacement of 72.0 mm), approximately 1.06 times higher than the P_{peak} value of the HC-24 specimen. The HC-50 specimen experiment ended because of a sharp load drop following the continuous fracture of the main

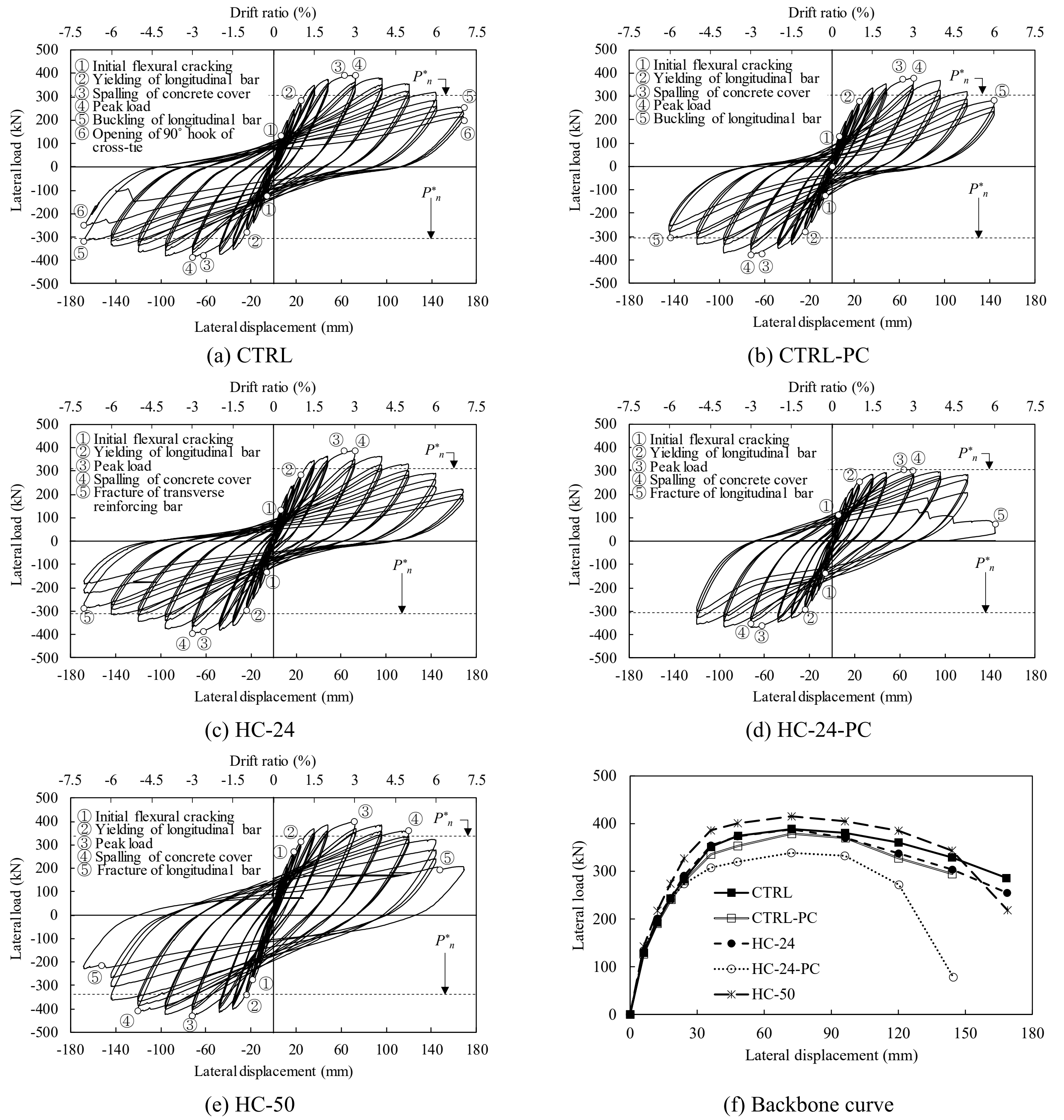

Fig. 8 Lateral load-displacement relationships of columns

reinforcement; the drift ratio was 7.0%, and the lateral load was 58% of P_{peak} or 241 kN. Furthermore, the rate of load decrease after the peak for HC-50 was more pronounced than that for the HC-24 specimen.

Fig. 8(f) shows the cyclic envelope curves of the specimens under positive loading. Upon examining the graph, the backbone curves of all five specimens aligned closely up to a drift ratio of 0.25% (displacement of 6 mm), indicating that the elastic behavior of the HPCC specimens was identical to that of the monolithic columns. Differences in the envelope curves of the HC-50 specimens began to appear after the drift ratio reached 0.5% (displacement of 12.0 mm). All specimens other than HC-50 showed almost identical behavior up to a drift ratio of 1.0% (displacement of 24.0 mm); however, beyond 1.0%, the rate of increase in HC-24-PC's backbone curve was measured as quite low. This pattern persisted among the specimens until they reached the peak load at the target drift ratio of 3.0% (displacement of 72.0 mm).

After the peak load, the load-reduction slopes of the HPCC specimens were steeper than those of the CTRL-series specimens. The structural integrity between the old and new concrete was compromised owing to continuous cracking and peeling in the external concrete in the descending phase. In contrast, the HC-24-PC specimen exhibited brittle behavior after the peak load compared to

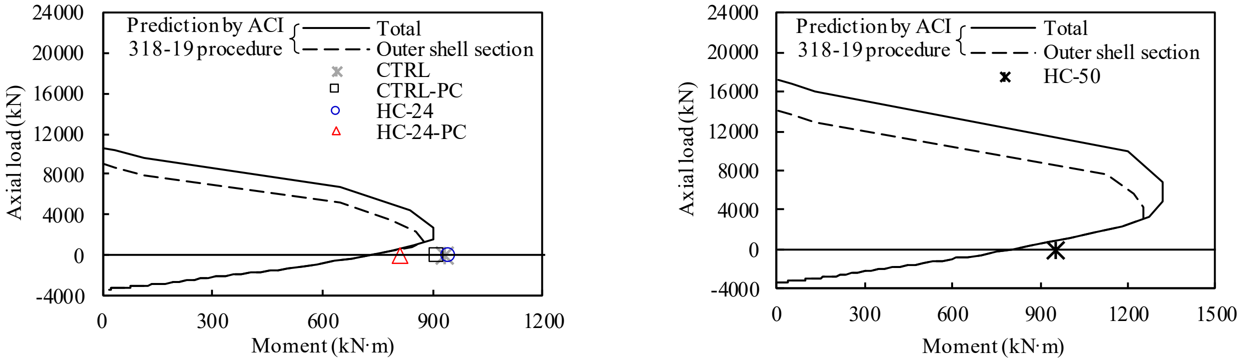

(a) Specimen with f'_c of 24 MPa (b) Specimen with f'_c of 50 MPa

Fig. 9 P-M interaction curve and measured maximum strength (P_{peak})

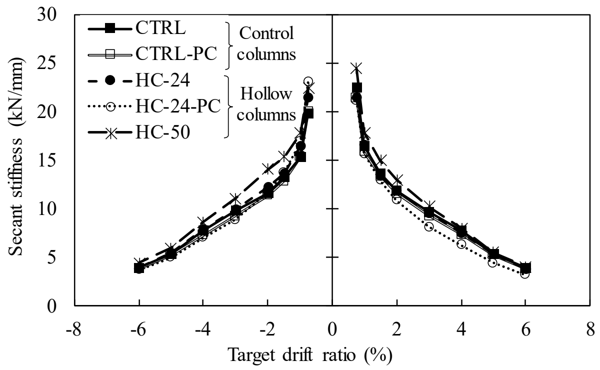

Fig. 10 Secant stiffness

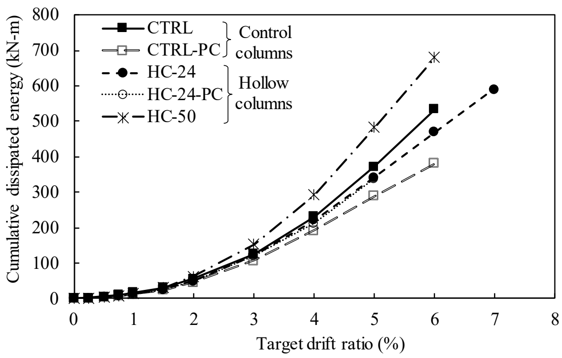

Fig. 11 Cumulative dissipated energy

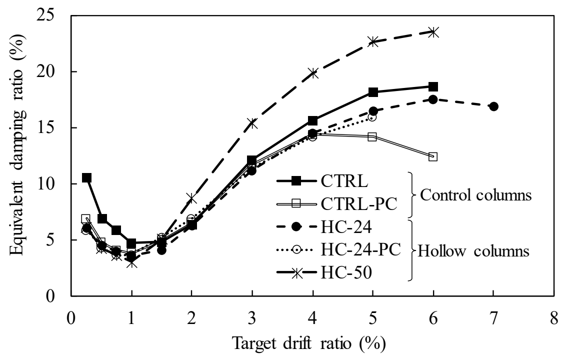

Fig. 12 Equivalent damping ratio

the other column specimens, believed to result from the stress concentration in the longitudinal bars beneath the sleeves. When comparing HC-24 and HC-50, which have different concrete strengths, the slope of the load reduction after the peak load exhibited a negligible influence on the compressive strength of the concrete because the volume ratio of the tie bars in HC-50 was set twice as high as that in HC-24 according to the design criteria (ACI 318-19 2019), ensuring a similar level of transverse reinforcement irrespective of the concrete compressive strength.

3.3 Moment capacity

The peak-measured moment strengths (M_{peak}) of the column specimens were compared with the predicted moment capacities according to ACI 318-19 (Table 4 and Fig. 9). In Fig. 9, the P-M curve for the outer shell was calculated excluding the hollow section, while the curve representing the total was derived by considering the gross section of the column, inclusive of the filled hollow section. The measured moment of each specimen was calculated by multiplying the measured peak load by the distance from the concrete base to the loading point. According to ACI 318-19, the ratio of M_{peak} to the predicted maximum moment (M^*_n) ranged from 1.11 to 1.28, slightly exceeding the predictions. All specimens had more than the amount of transverse reinforcement by ACI 318-19, suggesting that the ratio M_{peak}/M^*_n was conservatively estimated because of the confining effects of the concrete by the transverse reinforcement. Notably, the M_{peak} of the HC-24-PC specimen was approximately 1.06 times higher than the M^*_n, indicating that the hollow PC column meets the safety standards set by the design criteria.

3.4 Secant stiffness

To analyze the secant stiffness comparatively, the secant stiffnesses at the yielding ($K_y = P_y/\Delta_y$) and peak ($K_p = P_{peak}/\Delta_{peak}$) points were determined and are listed in Table 4. The secant stiffness trends for each specimen are shown in Fig. 10. K_y values for the CTRL and HC-24 specimens were 9.56 kN/m and 9.54 kN/m, respectively, with both registering a K_p value of 2.7 kN/m. Also, the K_y for the CTRL-PC and HC-24-PC specimens were 7.15 kN/m and 7.58 kN/m, respectively, and their K_p values were 2.64 and

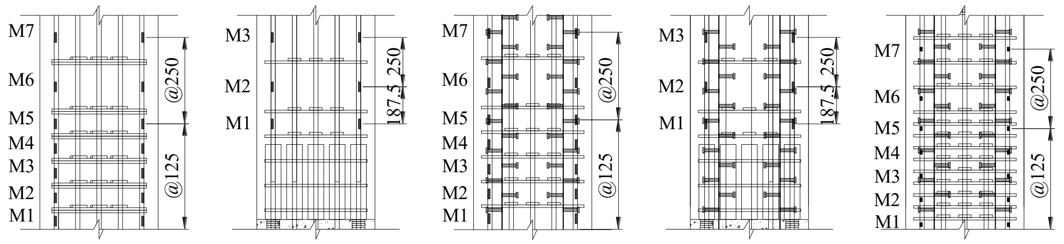

(a) Location of strain gauges

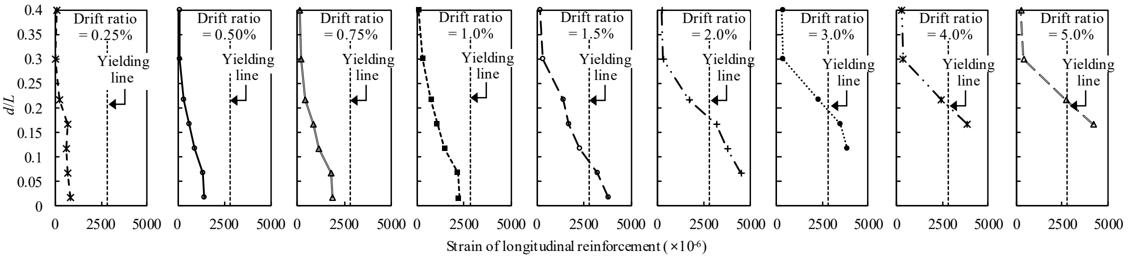

(b) CTRL

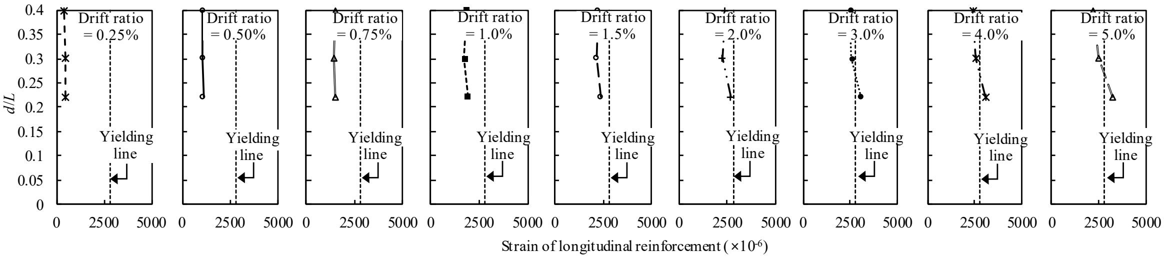

(c) CTRL-PC

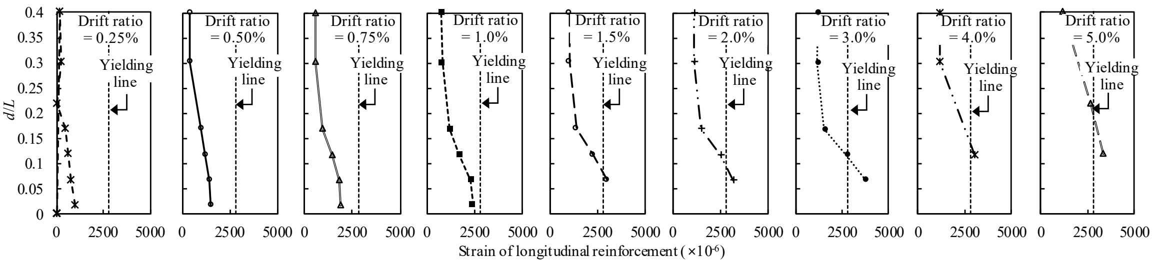

(d) HC-24

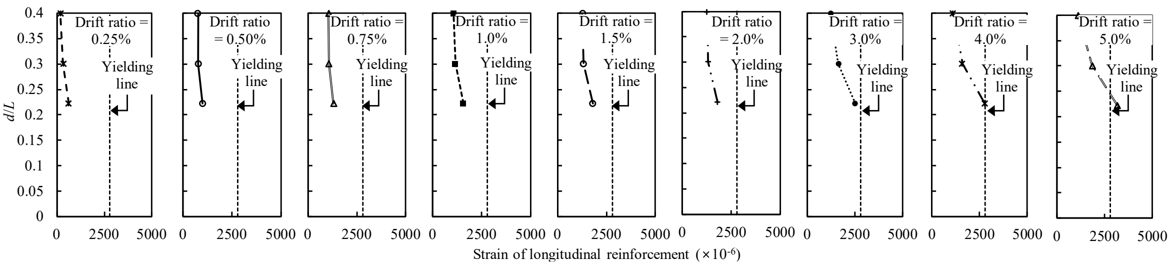

(e) HC-24-PC

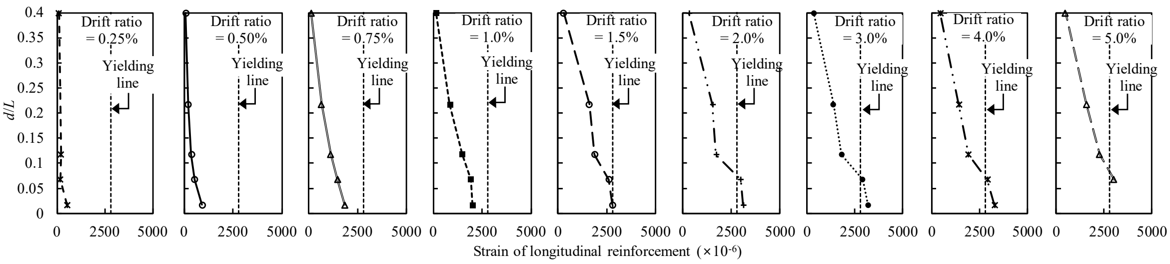

(f) HC-50

Fig. 13 Strain values of longitudinal bar at each target drift ratio

2.81 kN/m, making the stiffness of both specimens nearly identical. The K_y and K_p values for the HC-50 specimen were 8.32 kN/m and 2.63 kN/m, respectively, slightly lower than those of the HC-24 specimen. Overall, the secant stiffness trend with increasing loading was similar for all the specimens. From the perspective of secant stiffness, the stiffness of the HPCC specimens fabricated using the proposed technique was comparable to that of conventional RC columns.

3.5 Energy dissipation and equivalent damping ratios

Fig. 11 shows the cumulative dissipated energy (E_{acc}) of the specimens according to the target drift ratio. The energy dissipated in each cycle was equivalent to the enclosed area of the hysteresis loop of the cycle. Up to a target drift ratio of 3%, the E_{acc} values of all specimens were similar. Beyond a drift ratio of 3%, small variations in E_{acc} were observed among the specimens. At a target drift ratio of 5.0%, the E_{acc} of the CTRL specimen was 372.6 kN-m, approximately 16% higher than that of CTRL-PC. The E_{acc} of the HC-24 specimen was measured to be 342.9 kN-m, approximately 8% lower than the E_{acc} of the CTRL specimen. The E_{acc} of the HC-24-PC specimen was measured to be 338.9 kN-m, approximately 20% higher than the E_{acc} of the CTRL-PC specimen. Overall, the E_{acc} of the HC-24 and HC-24-PC specimens can be said to be similar to that of the CTRL/CTRL-PC specimens, owing to the high transverse confinement stress from the v-ties and the high integrity between the new and old concrete in the hollow PC columns, achieved using shear connectors and louver steel plates.

To equivalently assess energy dissipation, the specimens were evaluated for equivalent damping ratios, ξ_D (= $2A_{loop}/\pi A_{rec}$). Fig. 12 shows the ξ_D of the specimens according to the target drift ratio. where A_{loop} is the area of each cycle, and A_{rec} is the rectangular area calculated from the maximum/minimum displacement points of the cycle. From a target drift ratio of 0.25% to 1.5%, the ξ_D value of the CTRL specimen was higher than that of the other specimens. Up to a drift ratio of 1.5%, the ξ_D values for all specimens, except for the CTRL specimen, were similar. From a target drift ratio of 2% to 3%, the ξ_D values for all specimens, excluding the HC-50 specimen, were similar. At drift ratios of 4% and 5%, the ξ_D values for the CTRL specimen were 15.69 and 18.14, respectively, higher than those for the CTRL-PC, HC-24, and HC-24-PC specimens. The trend of ξ_D for the CTRL-PC specimen increased similarly to the CTRL specimen up to a drift ratio of 4% but dropped significantly after a drift ratio of 4%. Such a phenomenon is sometimes observed in PC specimens that use sleeves (Belleri and Riva 2012; Tullini and Minghini 2016, Yu *et al*. 2019). Conversely, the HPC-24-PC specimen showed similar ξ_D values to the HC-24 specimen up to a drift ratio of 5%. The ξ_D trend for the HC-50 specimen showed a significant increase compared to other specimens after a drift ratio of 1.5%, associated with the narrower spacing of the transverse confinement, which delayed the buckling of the main reinforcement and resulted in higher energy dissipation.

3.6 Displacement ductility ratio

To compare the ductility ratios of the specimens, the displacement ductility ratio (μ_Δ) proposed by Park and Paulay (1975) is determined by dividing the ultimate displacement (Δ_u) by the yielding displacement (Δ_y). The μ_Δ values for CTRL and CTRL-PC specimens were 4.72 and 3.61, respectively, indicating that the CTRL specimen possessed a higher value. The μ_Δ values for HC-24 and HC-24-PC specimens were 4.72 and 3.59, suggesting that the type of connection in which the column main reinforcement is directly connected to the foundation is superior. In other words, the ductility ratio of the specimens was significantly influenced by the connection type of the RC members. Comparing HC-24 and HC-50 specimens, the μ_Δ value of the HC-50 specimen, which used high-strength concrete, was relatively lower.

3.7 Strain distribution of longitudinal bars

To measure the strain of the main reinforcement in the specimens, the CTRL, HC-24, and HC-50 specimens were outfitted with seven strain gauges spaced at intervals of 125 mm for five and 250 mm for two from the concrete base (Fig. 13(a)). For the CTRL-PC and HC-24-PC specimens, three strain gages were installed on the main reinforcement in the upper part of the sleeve, as shown in Fig. 13(a). Figs. 13(b)-13(f) show the strain values in the rebars under tension when the specimens were subjected to positive loading. These values were normalized by dividing the distance at which the strain gauges were installed (in meters) by the column height (2400 mm). In the graphs, the dashed line represents the yielding strain, and the measured yielding strain value was 2600 μs. The main reinforcements in CTRL, HC-24, and HC-50 specimens not connected with the sleeves yielded at a target drift ratio of 1.5%. While the strain value below $0.2d/L$ for CTRL-PC and HC-24-PC specimens could not be measured, the gauge labeled M1 installed at the $0.2d/L$ point for CTRL-PC yielded a target drift ratio of 1.66%. Moreover, M1 for HC-24-PC yields a target drift ratio of 1.8%. Considering that the experiments with CTRL-PC and HC-24-PC ended because of the fracture of the longitudinal reinforcement, significant tensile forces may have been exerted on the dowel bars connected to the sleeves and yielded before reaching a drift ratio of 1.5%.

4. Conclusions

In this study, we propose a new inner mold that can form a hollow section to reduce the weight of precast columns. After using an inner mold fabricated from louver steel plates and L-channels to form the hollow section, we secured the structural integrity between the old and new concrete through louvers and shear studs. Quasi-static cyclic loading tests were performed to assess the seismic performance of precast concrete columns with hollow sections.

• The new prefabricated inner mold using a louver plate, shear studs, and V-ties was proposed for hollow precast concrete columns. The louver plate and shear studs act to secure integrity between the new and old concrete, while V-ties act to confine longitudinal bars instead of conventional transverse reinforcements. By using the new inner mold, we achieved a hollow ratio of 22%, resulting in a weight reduction of approximately 22% compared to monolithic columns. Because the amount of transverse reinforcement was greatly reduced, the overall weight of the HPCC was also relatively reduced compared to the CTRL, even considering the weight of the louver plates and shear studs.

The measured maximum strength (P_{peak}) of the hollow column specimens was nearly equivalent to that of the monolithic specimens, and in all scenarios, P_{peak} exceeded the strength predicted by ACI 318-19. In other words, the ACI 318 predictions aligned closely with the test results.

• The hysteresis behavior of the hollow column specimens was similar to that of the monolithic column specimens up to the peak moment; however, differences emerged after reaching the peak strength. Moreover, the hysteresis behavior after the peak strength in the precast concrete columns showed a greater reduction in load compared to the cast-in-place concrete column specimens. The PC specimens consistently ended the experiment at a drift ratio of 5.0–6.0%, more than 1% faster than that of the monolithic specimens, attributed to the localized stress concentration at the bottom of the longitudinal bars after P_{peak}, which deteriorated the load-transfer capacity.

• Excluding the HPCC specimens, the cumulative dissipated energy (E_{acc}) and equivalent damping ratio (ξ_D) of all the hollow column specimens were nearly identical to those of the monolithic columns up to a drift ratio of 2.0%. After a drift ratio of 3.0%, the E_{acc} and ξ_D values of the CTRL specimen were relatively superior to those of other specimens. Overall, up to the peak load (target drift ratio of 3%), the E_{acc} values for the columns with the formed hollow sections were nearly equivalent to those of the monolithic columns. However, after achieving the peak load, both E_{acc} and ξ_D values might exhibit a decline.

• The displacement ductility ratios of the HPCC specimens without spliced sleeves were similar to that of the CTRL. However, the displacement ductility ratio of the HPCC with spliced sleeves was lower than that of the CTRL. It is considered that the displacement ductility ratio is reduced when spliced sleeves are used.

• Upon evaluating the strain history of the longitudinal bars in each specimen, the strain values for each target drift ratio were consistent, regardless of the presence of a hollow section or a PC connection.

Acknowledgments

The work was supported by National Research Foundation of Korea (NRF) Grant (NRF-2021R1I1A2048618 and 2022R1A4A5028239).

References

ACI 374.2R-13 (2013), *Guide for Testing Reinforced Concrete Structural Elements Under Slowly Applied Simulated Seismic Loads*, American Concrete Institute; Farmington Hills, MI, USA.

ACI Committee 318 (2019), *Building Code Requirements for Structural Concrete (ACI 318-19) and Commentary*, American Concrete Institute; Farmington Hills, MI, USA.

ASTM C39/C39 M (2020), *Standard Test Method for Compressive Strength of Cylindrical Concrete Specimens*, ASTM International; PA, USA.

ASTM E8/E8 M (2016), *Standard Test Methods for Tension Testing of Metallic Materials*, ASTM International; PA, USA.

Belleri, A. and Riva, P. (2012), "Seismic performance and retrofit of precast concrete grouted sleeve connections", *PCI J.*, **57**(1), 97-109. https://doi.org/10.15554/pcij.01012012.97.109.

Hajdukiewicz, M., Goggins, J., Torre, O.D.L., Holleran, D. and Keane, M.M. (2019), "An automated standard-based life cycle quality inspection methodology for smart precast concrete solutions in buildings", *J. Struct. I. Maint.*, **4**(3), 123-134. https://doi.org/10.1080/24705314.2019.1627454.

Hao, J., Ren, Q., Li, X., Zhang, X., Ding, Y. and Zhang, S. (2022), "Experimental seismic behavior of RC special-shaped column to steel beam connections with steel jacket", *Steel Comp. Struct.*, **45**(1), 1259-1274. https://doi.org/10.12989/scs.2022.45.1.101.

Hwang, J.H., Lee, D.H., Oh, J.Y., Choi, S.H., Kim, K.S. and Seo, S.Y. (2016), "Seismic performances of centrifugally-formed hollow-core precast columns with multi-interlocking spirals", *Steel and Comp. Struct.*, **20**(6), 1259-1274. https://doi.org/10.12989/scs.2016.20.6.1259.

Im, C.R., Kim, S., Mun, J.H., Yang, K.H. and Sim, J.I. (2023b), "Push-out tests on headed studs and lattice shear connectors welded to louver steel plate", *Const. Build. Mater.*, **369**(6), 1-10. https://doi.org/10.1016/j.conbuildmat.2023.130528.

Im, C.R., Kim, S., Yang, K.H., Mun, J.H., Oh, J.H. and Sim, J.I. (2023a), "Cyclic loading test for concrete-filled hollow PC column produced using various inner molds", *Steel Comp. Struct.*, **46**(6), 793-804. https://doi.org/10.12989/scs.2023.46.6.793.

Jin, K., Yamazaki, K. and Takahashi, R. (2023), "Seismic performance of ductile column with rectangular hollow cross-section in RC building", *Appl. Sci.*, **13**(4), 1-22. https://doi.org/10.1016/j.conbuildmat.2023.130528.

Jung, D., Kang, T.H.K., Lee, D.J., Kim, S. and LaFave, J.M. (2023), "Seismic performance of a ductile rod exterior connection system for precast concrete industrial buildings", *PCI J.*, **8**(1), 28-47. https://doi.org/10.15554/pcij68.1-03.

Ke, X., Wei, H., Yang, L. and An, J. (2023), "Seismic performance and damage evaluation of concrete-encased CFST composite columns subjected to different loading systems", *Steel Comp. Struct.*, **47**(1), 121-134. https://doi.org/10.12989/scs.2023.47.1.121.

Kim, C.S., Lim, W.Y., Park, H.G. and Oh, J.K. (2016), "Cyclic loading test for cast-in-place concrete-filled hollow columns", *ACI Struct. J.*, **113**(5), 205-215. https://doi.org/10.14359/51688195.

Kim, S., Kang, T.H.K., Jung, D. and LaFave, J.M. (2021), "Seismic behavior of precast and post-tensioned exterior connections with ductile headed rods", *ACI Struct. J.*, **118**(1), 87-100. https://doi.org/10.14359/51728179.

Kim, W.W. and Yang, K.H. (2015), "Effect of bending angle and embedment length on the bond characteristics of V-shaped tie reinforcement", *J. Kor. Inst. Build. Const.*, **15**(5), 17-23. https://doi.org/10.5345/JKIBC.2015.15.5.465. (In Korean)

Park, R. and Paulay, T. (1975), *Reinforced Concrete Structures*. John Wiley & Sons, New Jersey, USA.

Tullini, N. and Minghini, F. (2016), "Grouted sleeve connections used in precast reinforced concrete construction – Experimental investigation of a column-to-column joint", *Eng. Struct.*, **127**, 784-803. https://doi.org/10.1016/j.engstruct.2016.09.021.

Wang, J.T., Wei, Y., Wang, J., Li, Y.W. and Sun, Q. (2023a), Seismic behavior of circular-in-square concrete-filled high-strength double skin steel tubular stub columns with out-of-code B/t ratios", *Steel Comp. Struct.*, **49**(4), 441-455. https://doi.org/10.12989/scs.2023.49.4.441.

Wang, X., Gao, P., Liu, J., Zhao, Q., Xu, H., Wei, W. and Wang, X.T. (2023b), "Assessment on seismic performance of circular concrete-filled thin-walled steel tube columns", *Adv. Struct. Eng.*, **26**(3), 399-412. https://doi.org/10.1177/136943322211288.

Yang, Y., Xue, Y., Yu, Y. and Gao, F. (2018), "Experimental study on seismic performance of partially precast steel reinforced concrete columns", *Eng. Struct.*, **175**, 63-75. https://doi.org/10.1016/j.engstruct.2018.08.027.

Yu, Z., Lv, X., Yu, Y., Ding, F. and Peng, X. (2019), "Seismic performance of precast concrete columns with improved U-type reinforcement ferrule connections", *Inter. J. Concr. Struct. Mater.*, **13**(54), 1-18. https://doi.org/10.1186/s40069-019-0368-6.

CC